Ferroelectric–carbon nanotube memory devices

2012 Nanotechnology 23 165702

(http://iopscience.iop.org/0957-4484/23/16/165702)

Nanotechnology **23** (2012) 165702 (6pp) doi:10.1088/0957-4484/23/16/165702

Ferroelectric–carbon nanotube memory devices

Ashok Kumar[1,2], Sai G Shivareddy[3], Margarita Correa[1], Oscar Resto[1], Youngjin Choi[3], Matthew T Cole[3], Ram S Katiyar[1], James F Scott[1,4], Gehan A J Amaratunga[3], Haidong Lu[5] and Alexei Gruverman[5]

[1] Department of Physics and Institute for Functional Nanomaterials, University of Puerto Rico, San Juan, PR 00936-8377, USA
[2] National Physical Laboratory, New Delhi, 110012, India
[3] Electrical Engineering Division, Department of Engineering, University of Cambridge, Cambridge CB3 OFA, UK
[4] Department of Physics, Cavendish Laboratory, University of Cambridge, Cambridge CB3 OHE, UK
[5] Department of Physics and Astronomy, University of Nebraska, Lincoln, NE 68588, USA

E-mail: ashok553@gmail.com, jfs32@hermes.cam.ac.uk and gaja1@hermes.cam.ac.uk

Received 1 February 2012, in final form 2 March 2012
Published 30 March 2012
Online at stacks.iop.org/Nano/23/165702

Abstract
One-dimensional ferroelectric nanostructures, carbon nanotubes (CNT) and CNT–inorganic oxides have recently been studied due to their potential applications for microelectronics. Here, we report coating of a registered array of aligned multi-wall carbon nanotubes (MWCNT) grown on silicon substrates by functional ferroelectric Pb(Zr, Ti)O_3 (PZT) which produces structures suitable for commercial prototype memories. Microstructural analysis reveals the crystalline nature of PZT with small nanocrystals aligned in different directions. First-order Raman modes of MWCNT and PZT/MWCNT/n-Si show the high structural quality of CNT before and after PZT deposition at elevated temperature. PZT exists mostly in the monoclinic *Cc*/*Cm* phase, which is the origin of the high piezoelectric response in the system. Low–loss square piezoelectric hysteresis obtained for the 3D bottom-up structure confirms the switchability of the device. Current–voltage mapping of the device by conducting atomic force microscopy (c-AFM) indicates very low transient current. Fabrication and functional properties of these hybrid ferroelectric–carbon nanotubes is the first step towards miniaturization for future nanotechnology sensors, actuators, transducers and memory devices.

(Some figures may appear in colour only in the online journal)

1. Introduction

The combination of carbon nanotubes and ferroelectric oxides into a single nanodevice has been appealing for the past decade: ferroelectric, pyroelectric and piezoelectric devices on the nanoscale could provide new paradigms for memory applications, for medical implants, and for aerospace applications where space and weight are at a premium. The combination is of great advantage for two reasons: carbon nanotubes are superb interconnects, but in order to produce new device systems they must have functional end groups, such as piezoelectric transducers, pyroelectric detectors or binary memory storage cells at their ends. Conversely, ferroelectrics initially made a significant commercial entry as memories in the Sony Playstation 2 but have not followed up that early success in rapid commercialization in part because they could not meet the rapidly decreasing size requirements of their underlying Si circuitry (at present the 22 nm node). During the last two decades carbon-based functional nanostructures (carbon nanotubes (CNT—multi-wall, single-wall, bamboo-like), monolayer graphene, graphene oxide, nanocrystalline diamond) have been widely investigated due to their extraordinarily high mechanical, thermal, electrical and corrosion-resistant properties [1, 2]. Inorganic ferroelectric materials are also well established as nonvolatile random access memories (NVRAM), microelectromechanical systems (MEMS) and nano-NEMS-based sensors and actuators, radio-frequency identification (RFID) tags and

other applications [3, 4]. Devices based on either organic or inorganic nanomaterials have to follow Moore's law in order to meet the International Technology Roadmap for Semiconductors (ITRS) criteria for future memory and sensor applications. To meet the 22 nm node for future technology, the physical dimension of the ferroelectric oxides should be significantly reduced, which in turn makes it more challenging in terms of device reliability [5]. Due to large leakage current and insufficient amount of switchable charge, ferroelectric memory faces a dimensionality problem: the device is not reliable for less than 120–180 nm diameters. To overcome these problems one has either to find ferroelectric materials with extraordinarily high switchable charge below 100 nm width or design some (3D) structures which yield very high surface areas. Ferroelectric materials are facing similar problems for NEMS/MEMS applications: with the reduction of size their mechanical strength is significantly reduced, which again puts a question mark on their reliability. Note that it is the 'footprint' on the integrated circuit that is the size limitation; (3D) structures maintain large surface areas (and hence large switched charge for sense amplifiers and discriminators to read) while minimizing the footprint.

Several researchers have emphasized over the past four years the possibility of making functional devices such as electrical switches and memories by means of functional nanomaterials connected by carbon nanotubes (CNTs). One of the most promising of these was the LSCO/CNT (lanthanum strontium cobaltate) device of Hueso *et al* [6]. Subsequently partial successes were reported by Miyake *et al* [7] and Kawasaki *et al* [8, 9] in putting ferroelectric nanotips onto CNTs, but switching was demonstrated on only bare ferroelectric nanotubes [7] and not on those connected via CNTs [9, 10]. Paruch *et al* showed polarization switching using single-walled carbon nanotubes grown on epitaxial ferroelectric thin films [11], but these observations were not followed up or developed into real devices. In the present work we extend the single-walled CNT work of Paruch *et al* to multi-walled CNTs and demonstrate functional parameters suitable for real devices. In addition, our CNT–FE devices are vertically aligned, making their large-area addressing feasible, unlike studies in which single CNTs in plane were probed. All ferroelectric nanotubes pose a problem in terms of contacts to achieve optimal polarization along the axis of the tube. This problem can be solved by having the ferroelectric nanotube hollowed out along its axis and filling the space with a contact, with the complete functional structure achieved by coating the CNT with ferroelectric material. The deposition of ferroelectrics tips onto CNTs is a rather subtle process, because oxide ferroelectrics require high-temperature deposition in oxygen ambient, whereas CNTs can simply ignite under such conditions. We have used expertise gained in the growth of registered arrays of CNT (multi, single, bamboo) on silicon substrates by PECVD utilizing well-defined Ni catalyst placement to control the pitch, height, diameter and inner wall thickness of the CNTs for ferroelectric coating [12, 13].

We report a functional nanoferroelectric switch utilizing carbon nanotubes as interconnects. We visualize ferroelectric nanodomains via piezoresponse force microscopy (PFM) [14], demonstrate switchability by acquiring local PFM hysteresis loops and characterize current–voltage (*IV*) properties of the integrated nanodevices by means of conducting atomic force microscopy (c-AFM). One of the major challenges in nanoscale science is the control (pitch, height, diameter) and synthesis of nanomaterials with monodisperse size, uniform morphologies and functionalized surfaces. For potential electronic applications, such as nanoscale NVRAM, nanocapacitors, NEMS, energy-harvesting devices, photocatalysts, etc, the controlled addressing and assembling of large arrays of nanostructures is necessary [15, 16]. A topical review on one-dimensional nanostructure ferroelectrics [14] and carbon nanotube–inorganics (mostly non-ferroelectric oxides) has covered almost all of the state-of-the-art development in these hybrid structures [16]. A literature survey of CNT–ferroelectric hybrid structures indicates only a handful of publications due to the complexity of phase formation at high temperature [4, 6, 17]. Our work is a first step towards the control of growth and functional property over large-area Si substrates. If these devices are to be successful, it would help by downsizing the technology by at least an order of magnitude, and to provide cheap, environmentally friendly direct connection with Si-based technology.

2. Experimental details

Registered arrays of MWCNTs were grown in a highly oriented manner on n-Si by a method reported in detail elsewhere [18]. Patterning of Ni catalyst dots on Nb was done utilizing e-beam lithography with a lift-off technique on the large area of Si substrate. Plasma-enhanced chemical vapor deposition (PECVD) was used for CNT growth utilizing acetylene (C_2H_2) (for CNT growth) and ammonia (NH_3) (to etch the unwanted amorphous carbon) gases. The growth of MWCNTs takes place at 700 °C in the presence of these precursor gases C_2H_2 and NH_3 gases. The length of the nanotubes depends on the growth time, whereas the Ni catalyst dot diameter determines the CNT diameter. Vertical alignment of the nanotubes was achieved through the electric field induced during DC plasma growth. In the present case, we have used a highly dense, lower pitch alignment, 1–3 μm in length and forest-like MWCNT structure, as seen in the large-area scanning electron microscopy (SEM) image of devices (figures 1(b) and (d)). A Pb-rich $Pb(Zr_{0.52}Ti_{0.48})O_3$ (PZT) target was prepared by a conventional solid-state reaction method for the deposition of the nanoferroelectric onto MWCNTs by a pulsed-laser deposition (PLD) technique [19]. Low laser frequency (5–7 Hz), moderate laser energies (1–2 J cm^{-2}), low oxygen atmospheres of (70–80 mTorr) and reasonably high temperatures (500–550 °C) were employed to get the crystalline films on MWCNTs utilizing a KrF excimer laser ($\lambda = 240$ nm). After the deposition of the PZT film, the chamber was cooled at a rate of 10 K min^{-1} until 300 °C and subsequently 5 °C min^{-1} until room temperature in an oxygen atmosphere at 300 Torr.

Electrical testing of the PZT–CNT nanostructures has been performed using a commercial atomic force microscope

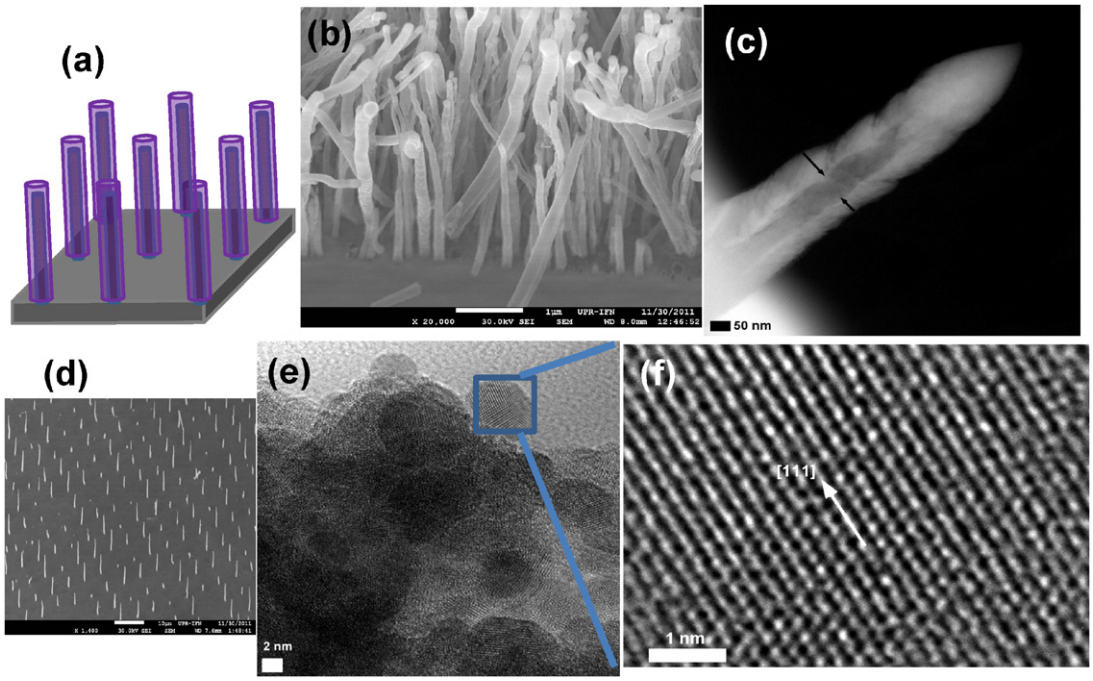

Figure 1. (a) Sketch diagram of devices. Registered array of MWCNTs are grown on n-Si substrate by PECVD technique. (b) Large-area SEM image of the dense forest PZT/MWCNT/n-Si heterostructure suggests conformal coating on the function PZT, (c) single PZT/MWCNT nanotubes, 100–150 nm in diameter after coating, 1–5 μm in length, (d) well-aligned conformally coated PZT/MWCNT/n-Si heterostructure; pitch, dimensions and length depend upon the growth catalyst (Ni) and growth conditions. (d) TEM image of PZT nanocrystals at the outer edge of the CNTs and (e) HRTEM image showed the lattice plane of (111) plane.

(Asylum MFP-3D). Bias-off PFM local switching loops were obtained as a function of dc switching pulses superimposed on ac modulation bias. Typical frequency range for an ac voltage was 300–350 kHz with amplitude of 0.8 V (peak-to-peak). Conductive Pt-coated silicon cantilevers (NSC18/Pt, Mikromasch) were used for the measurements.

Nanoscale spatially resolved electrical transport measurements have been performed using c-AFM by positioning a conductive diamond tip (CDT-NCHR, Nanoworld) at a selected point on the film surface and measuring local current–voltage characteristics. Current maps were obtained simultaneously with the topographic data by scanning the surface with the tip held under a constant dc bias at 1 V and measuring current at each pixel point of the scanned area.

Scanning electron microscopy images were obtained with a high-resolution field emission SEM model JSM-7500F from JEOL. Transmission electron microscope studies were carried out with a high-resolution Cs probe-corrected JEOL JEM-2200FS TEM.

3. Results and discussion

A schematic diagram in figure 1(a) shows our approach of a (3D) CNT bottom electrode connected to a Si substrate with conformally coated functional ferroelectric end caps. The final step is the conformal metallization of the ferroelectric surface to exploit the maximum functional surface area. This approach has been successfully employed for high-k oxides, often considered as low-leakage materials, which have shown tremendous potential for nanoscale capacitors and electromechanical systems [12, 15, 18, 20]. Figure 1(b) shows an SEM image of the PZT-coated forest-like MWCNT nanotubes. The density of the coated nanotubes is quite large: average dimensions are 100–150 nm (diameter) and 2–4 μm long. The density and dimensions of the coated nanotubes depend upon the PECVD growth conditions and on the Ni catalyst dots. The mechanism of nanotube growth in these experiments is a tip-type growth with the Ni catalyst at the tip of the nanotube which produces closed capped tubes that have a higher activation energy barrier for oxidation [18, 19] . It is worth mentioning that it is the quality of CNTs which plays the vital role in the final structure, as can be seen in figure 2(d) where all the CNTs are coated conformably with PZT and well aligned over a large area. Conformal coating of PZT for all the CNTs is observed without any significant degradation in the electrical and physical properties that will be discussed in the Raman and AFM section below. Kawasaki *et al* report the conformal coating of PZT on CNT by a chemical solution deposition technique; they found a very narrow temperature window (220–250 °C) for successful coating and raised concerns about oxidation of the nanotubes at elevated temperatures [10]. At temperatures (above 500 °C) required in typical PLD processes, nanotube oxidation is expected. However, the exact temperature at which the PLD process does not produce good results would depend on oxygen partial pressure during the process and the physical structure of the nanotube, like the number of graphene walls, aspect ratios, mechanical strength, impurities and chemical instabilities. Further studies of factors affecting the deposition will be reported elsewhere [15]. Previous oxidation studies of MWCNTs by Ajayan *et al* [21] show that their oxidation reaction follows an Arrhenius-type

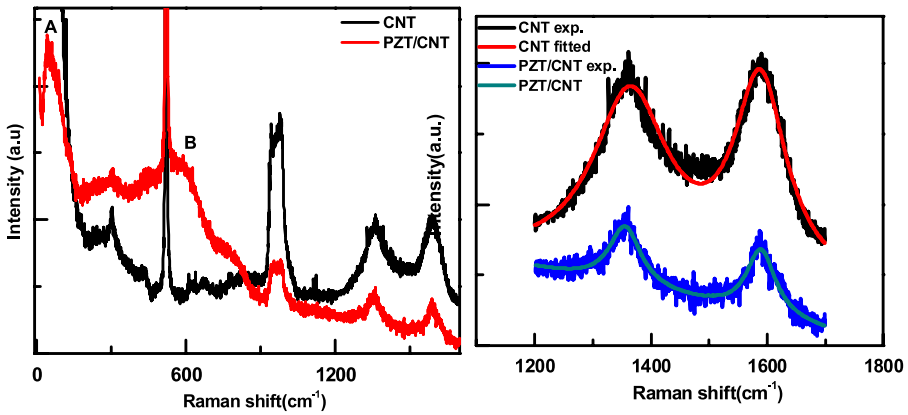

Figure 2. Room temperature micro-Raman spectra of MWCNTs (black line with high intensity of CNT D and G modes) and PZT/MWCNTs (low intensity), lowest 48 cm^{-1} mode belong to PZT, high intensity near B is mainly due to higher order E (LO) and A(TO) modes of PZT in 500–600 cm^{-1} regions. Close look of MWCNT Raman spectra (right-hand side), D and G bands of MWCNT experimental and theoretical (continuous line, fitted with damped harmonic oscillator phonon model ([22]) Raman spectra.

dependence on temperature with an activation energy barrier of about 225 kJ mol^{-1}. The nanotube caps begin to open at temperatures beyond 700 °C and oxidation rapidly occurs, with the outer graphene layers peeling off layer by layer, resulting in the thinning of the MWCNTs.

4. Transmission electron microscopy (TEM)

High-resolution transmission electron microscopy (HRTEM) images of individual nanotubes and especially the peripheral region of the PZT/MWCNT nanotubes are shown in figures 1(c) and (e), respectively. Figure 1(c) provides direct evidence of the formation of the hybrid structure; it shows a MWCNT of ∼80 nm diameter covered by a 50–80 nm PZT layer. Small nanocrystals of PZT with average sizes 2–5 nm are seen with different crystal orientations (figure 1(e)); even the small individual nanocrystals have different orientations, and these nanocrystals also show dynamic behavior under constant e-beam energy. The dynamic behavior of the crystal may be due to localized heat generated by e-beams which, in turn, changes the crystal orientations and sometimes their crystallographic phases. Detailed dynamics of these nanocrystals will be discussed elsewhere. However, owing to the strong dependence of the Bethe–Bloch cross section for electron–electron interaction on electron velocity, the damage rate can be substantially reduced by increasing the operating voltage to 400 kV [22]. Mapping of the atomic positions and lattice planes of our nanocrystals is shown in figure 1(f). The distance between the (111) plane is 2.355 Å and matches well with the crystal structure of ultra-thin PZT films [23]. Apart from the well-defined lattice plane, we have also observed inhomogeneity in the nanocrystals and surrounding area. Raman spectra of PZT/MCNT also show the presence of F_{2g} modes (not soft, and implying the localization of Pb–O bonding) similar to the chemically inhomogeneous microstructure of relaxor ferroelectrics [24].

5. Raman studies

Microstructural analysis of PZT/MWCNT confirms the conformal coating of PZT on MWCNT. One question still remains—whether the CNTs exist with all the electrical, chemical and mechanical properties after deposition? For a direct answer to this question, one needs very thin layers of PZT (<10–15 nm) on CNTs with cross-sectional cut by focused-ion beams, and finally HRTEM to see the cross-sectional image for the positions of carbon layers and perovskite. We are working on this challenging task currently to see the atomic scale bonding near the interface of PZT and CNT. Although the dark-field imaging of PZT/MWCNT in the STEM mode showed a clear picture of the CNT core with well-defined (3D) coating of PZT, this result is a significant step towards direct evidence of the existence of CNT after deposition. Raman spectra, which are known as 'fingerprints' for carbon and/or oxide materials, ruled out degradation of CNT after deposition. First-order micro-Raman spectroscopy studies have been performed on MWCNT/n-Si and PZT/MWCNT/n-Si nanostructures (figures 2(a) and (b)). The nature of Raman modes of MWCNT before and after PZT deposition indicates the following facts, also shown in figure 2(b): (i) two prominent peaks at high frequency around 1355 cm^{-1} (D band) and 1588 cm^{-1} (G band) due to the presence of sp^2–sp^3 carbon structures; (ii) a small upward shift (∼10 cm^{-1}) in D-band energy after deposition; (iii) decrease in full width at half-maximum (FWHM) after PZT coating; and (iv) intensity of both modes are almost the same. Two well-defined MWCNT peaks at 1588 cm^{-1} and the second-strongest band at 1355 cm^{-1} could be attributed to the fundamental frequency modes E_{2g} and D (induced by defects) analogous to those of graphite [25].

6. Theory

Group theory predicts 27 Raman-active modes for the monoclinic *Cc* model of $PbZr_{1-x}Ti_xO_3$ $(0 < x1)$ $13A' + 14A''$, and 11 active modes for the rhombohedral *R*3*c* model $4A_1 + 7E$. However, for the other structures, 12 active modes are predicted for the monoclinic *Cm* model $7A' + 5A''$ and 7 for the rhombohedral *R*3*m* model $3A_1 + 4E$. For the compositions above the morphotropic phase boundary

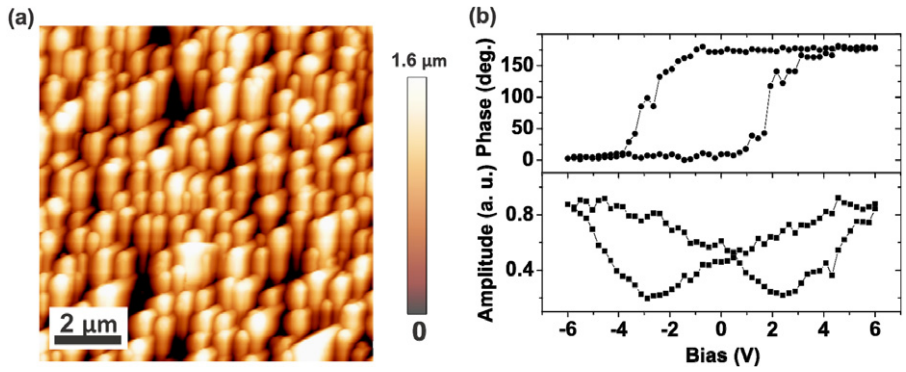

Figure 3. (a) Surface topography of PZT/MWCNT indicates well-aligned and dense hybrid structure, (b) PFM hysteresis loops detected in an individual PZT/MWCNT indicating nanoscale switching behavior.

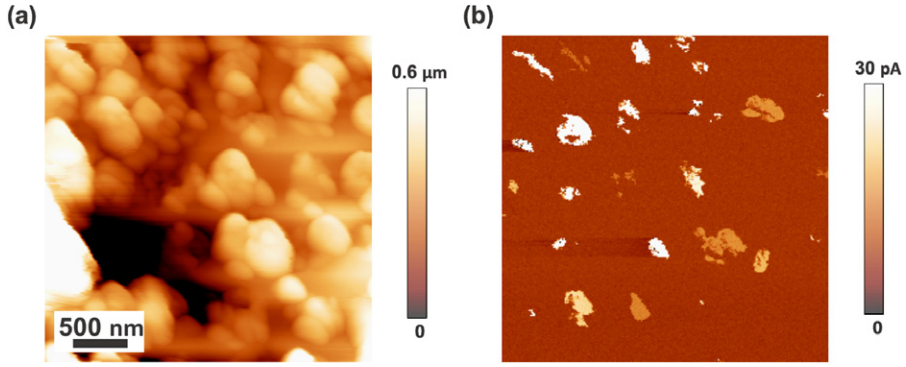

Figure 4. (a) Surface topography of hybrid structure and (b) corresponding current mapping under 1 V dc. Bright area indicates good transient current response.

(MPB) and near to $PbTiO_3$ there is a ferroelectric tetragonal *P*4*mm* phase [26–29]. Raman spectra of the morphotropic phase boundary are complicated and hard to assign for any particular crystal system. Noheda *et al* discovered the monoclinic phase near the MPB ($0.45 < x < 0.66$) which was considered as a derivative from both tetragonal and rhombohedral phases [26, 27]. Lima *et al* did a detailed Raman study for the compositions of PZT near the MPB at low temperature and found interesting low-frequency Raman-active modes (~40–60 cm^{-1}) similar to F_{2g} modes of relaxor ferroelectrics in the monoclinic phase [22, 27]. In the present study such a low-frequency active Raman mode (~48 cm^{-1}) is observed at room temperature (marked A in figure 2). The shift and presence of this low-lying mode is mainly due to three-dimensional strains. We believe that most of the PZT in the present case exists in the monoclinic phase of PZT, which is very good for functional properties. As we know the high piezoelectric response in the PZT system is due to the presence of a monoclinic phase which is very much needed for device applications [27]. The other Raman-active modes of PZT are dominated by sharp n-Si substrate peaks in the same regions. It is interesting to note that region B in figure 2 has very high intensity compared to the substrate. It would be unwise to assign the PZT peaks due to the high background of the substrate. In summary, Raman spectra confirm the crystalline phase of PZT at the nanoscale, the presence of MWCNT after PZT deposition and the quality of MWCNT of the hybrid structure.

7. Ferroelectric switching and nanoscale conduction mapping

Figure 3(a) shows a topographic image of a structure of densely packed well-aligned PZT/MWCNT nanotubes. Local PFM hysteresis loops [30–34] measured on an individual PZT–CNT reveal a behavior typical for ferroelectric polarization switching. Multiple PFM measurements (>100 curves) performed at various locations showed significant point-to-point variability of the local coercive voltage. Spatial variations in physical properties of the PZT/MWCNT structure have also been observed during nanoscale measurements of the local transport behavior by means of conducting atomic force microscopy (c-AFM). A leakage current map has been obtained simultaneously with the topographic image by scanning the surface with the tip held under a constant dc bias and detecting current at each pixel (figure 4). Nanoscale current mapping revealed strong variations in local conductivity: brighter regions seen on the dark background correspond to PZT–CNT elements with higher conductivity. The reason for such a different behavior is not clear. Possible reasons include defect structure of the PZT grains, variations in the transport properties of individual nanotubes

and variability in the contact resistance of PZT/MWCNT junctions (most likely).

8. Summary

Large-area functional ferroelectric-coated vertically registered CNTs are fabricated on silicon as a basis for scaling of future technology. SEM and TEM analysis verify conformal coating of PZT on CNT with high crystalline quality. Raman spectra of CNTs before and after functional oxide coating at elevated temperature display almost similar phonon frequencies and lineshapes, indicating that the CNTs retain their pre-coating structure. Nanoscale switching is observed with square hysteresis behavior and butterfly loops. $I(V)$ mapping over large areas showed low transient current. This (3D) hybrid bottom-up (CNT array formation) and top-down (PZT ferroelectric structure) approach provides a route to miniaturization of ferroelectric structures for the microelectronics industry.

Acknowledgments

This work was partially supported by the EPSRC UK and Dyson Research (at Cambridge), W911NF-06-1-0183, W911NF1110204 and DoE FG 02-08ER46526 grants.

References

[1] Awano Y, Sato S, Nihei M, Sakai T, Ohno Y and Mizutani T 2010 Carbon nanotubes for VLSI: interconnect and transistor applications *Proc. IEEE* **98** 2015–31
[2] Iijima S 1991 Helical microtubules of graphitic carbon *Nature* **354** 56–8
[3] Scott J F and Araujo C A P 1989 Ferroelectric memories *Science* **246** 1400–5
[4] Bedekar V, Murayama M, Mahajan R L and Priya S 2010 Controlled synthesis of $BaTiO_3$-coated multiwall carbon nanotubes *J. Am. Ceram. Soc.* **93** 3618–23
[5] www.itrs.net/Links/2010ITRS/2010Update/ToPost/ERD_ERM_2010FINALReportMemoryAssessment_ITRS.pdf
[6] Hueso L E, Pruneda J M, Ferrari V, Burnell G, Valdes-Herrera J P, Simons B D, Littlewood P B, Artacho E, Fert A and Mathur N D 2007 Transformation of spin information into large electrical signals using carbon nanotubes *Nature* **445** 410–3
[7] Miyake M, Scott J F, Lou X J, Morrison F D, Nonaka T, Motoyama T and Tsuji O 2008 Submicron three-dimensional trenched electrodes and capacitors for DRAMs and FRAMs: fabrication and electrical testing *J. Appl. Phys.* **104** 064112
[8] Luo Y, Szafraniak I, Zakharov N D, Nagarajan V, Steinhart M, Wehrspohn R B, Wendorff J H, Ramesh R and Alexe M 2003 Nanoshell tubes of ferroelectric lead zirconate titanate and barium titanate *Appl. Phys. Lett.* **83** 440–2
[9] Scott J F *et al* 2008 THz emission from tubular Pb(Zr, Ti)O_3 nanostructures *Nano Lett.* **8** 4404–9
[10] Kawasaki S *et al* 2008 Conformal oxide coating of carbon nanotubes *Appl. Phys. Lett.* **92** 053109
[11] Paruch P, Posadas A-B, Dawber M, Ahn C H and McEuen P L 2008 Polarization switching using single-walled carbon nanotubes grown on epitaxial ferroelectric thin films *Appl. Phys. Lett.* **93** 132901
[12] Spanier J E, Kolpak A M, Urban J J, Grinberg I, Ouyang L, Yun W S, Rappe A M and Park H 2006 Ferroelectric phase transition in individual single-crystalline $BaTiO_3$ nanowires *Nano Lett.* **6** 735
[13] Jang J E, Cha S N, Choi Y J, Kang D J, Butler T P, Hasko D G, Jung J E, Kim J M and Amaratunga G A J 2008 Nanoscale memory cell based on a nanoelectromechanical switched capacitor *Nature Nano* **3** 26–30
[14] Gruverman A and Ikeda Y 1998 Characterization and control of domain structure in $SrBi_2Ta_2O_9$ thin films by scanning force microscopy *Japan. J. Appl. Phys.* **37** L939
[15] Shivareddy S G, Kumar A, Choi Y, Lee G, Choi H, Hong S, Katiyar R S, Scott J F and Amaratunga G A J 2012 Carbon nanotubes as interconnects for functional nano-ferroelectrics, private communication
[16] Rørvik P M, Grande T and Einarsrud M A 2011 One-dimensional nanostructures of ferroelectric perovskites *Adv. Mater.* **23** 4007–34
[17] Dominik E 2010 Carbon nanotube-inorganic hybrids *Chem. Rev.* **110** 1348–85
[18] Choi Y, Mosley L E, Min Y and Amaratunga G A J 2011 Carbon nanotube capacitors arrays using high-k dielectrics *Diamond Relat. Mater.* **19** 221–4
[19] Ortega N, Kumar A, Bhattacharya P, Majumder S B and Katiyar R S 2008 Impedance spectroscopy of multiferroic $PbZr_xTi_{1-x}O_3/CoFe_2O_4$ layered thin films *Phys. Rev.* B **77** 014111
[20] Teo K B K *et al* 2003 Plasma enhanced chemical vapour deposition carbon nanotubes/nanofibres how uniform do they grow? *Nanotechnology* **14** 204–11
[21] Ajayan P M, Ebbesen T W, Ichihashi T, Iijima S, Tanigaki K and Hiura H 1993 Opening carbon nanotubes with oxygen and implications for filling *Nature* **362** 522–5
[22] Williams D B and Carter C B 1996 *Transmission Electron Microscopy* (New York: Plenum)
[23] Jia C L, Nagarajan V, He J Q, Houben L, Zhao T, Ramesh R, Urban K and Waser R 2007 Unit-cell scale mapping of ferroelectricity and tetragonality in epitaxial ultrathin ferroelectric films *Nature Mater.* **6** 64–9
[24] Correa M, Kumar A, Priya S, Katiyar R S and Scott J F 2011 Phonon anomalies and phonon-spin coupling in oriented $PbFe_{0.5}Nb_{0.5}O_3$ thin films *Phys. Rev.* B **83** 014302
[25] Zhang H B, Lin G D, Zhou Z H, Dong X and Chen T 2002 Raman spectra of MWCNTs and MWCNT-based H—adsorbing system *Carbon* **40** 2429
[26] Noheda B, Cox D E, Shirane G, Gonzalo J A, Park S E and Cross L E 1999 A monoclinic ferroelectric phase in the $Pb(Zr_{1-x}Ti_x)O_3$ solid solution *Appl. Phys. Lett.* **74** 2059
[27] Noheda B, Gonzalo J A, Cross L E, Guo R, Park S-E, Cox D E and Shirane G 2000 Tetragonal-to-monoclinic phase transition in a ferroelectric perovskite: the structure of $PbZr_{0.52}Ti_{0.48}O_3$ *Phys. Rev.* B **61** 8687
[28] Guo R, Cross L E, Park S-E, Noheda B, Cox D E and Shirane G 2000 Origin of the high piezoelectric response in $PbZr_{0.52}Ti_{0.48}O_3$ *Phys. Rev. Lett.* **84** 5423
[29] Lima K C V, Souza Filho A G, Ayala A P, Filho J M, Freire P T C and Melo F E A 2001 Raman study of morphotropic phase boundary in $PbZr_{1-x}Ti_xO_3$ at low temperatures *Phys. Rev.* B **63** 184105
[30] Durkan C, Chu D, Migliorato P and Welland M E 2000 Investigations into local piezoelectric properties by atomic force microscopy *Appl. Phys. Lett.* **76** 366
[31] Hong S, Woo J, Shin H, Jeon J U, Pak Y E, Colla E, Setter N, Kim E and No K 2001 Principle of ferroelectric domain imaging using atomic force microscope *J. Appl. Phys.* **89** 1377
[32] Kalinin S V and Bonnell D A 2002 Imaging mechanism of piezoresponse force microscopy of ferroelectric surfaces *Phys. Rev.* B **65** 125408
[33] Gruverman A and Kholkin A 2006 Nanoscale ferroelectrics: processing, characterization and future trends *Rep. Prog. Phys.* **69** 2443–74
[34] Alexe M and Gruverman A 2004 *Ferroelectrics at Nanoscale: Scanning Probe Microscopy Approach* ed M Alexe and A Gruverman (Berlin: Springer)